1	Dueling backbones: comparing peptoid and peptide analogs of a mussel
2	adhesive protein
3	
4	William R. Wonderly <sup>1†</sup> , Thomas R. Cristiani <sup>1‡</sup> , Keila C. Cunha <sup>1†</sup> , George D. Degen <sup>§</sup> ,
5	Joan E. Shea <sup>†,¶</sup> , J. Herbert Waite* <sup>†,ß</sup>
6	† Danautus aut of Chamistus (2. Diaghamistus)
7 8	† Department of Chemistry & Biochemistry,  † Materials Department
9	§ Department of Chemical Engineering,
10	¶Department of Physics
11	<sup>®</sup> Biomolecular Science & Engineering Program,
12	University of California Santa Barbara, Santa Barbara, CA, 93106
13	
14	1
15 16	<sup>1</sup> contributed equally
17	
18	<ul> <li>Corresponding authors: (JHW) <u>hwaite@ucsb.edu</u></li> </ul>
19	(JES) shea@ucsb.edu
20	ORCID
21	J Herbert Waite: 0000-0003-4683-7386
22	Joan Emma Shea: 0000-0002-9801-9273
23	

# **ABSTRACT**

1 2

3

4

5

6

7

8

9

10

11

12

13

14

15

16

17

Ensembles of amino acid side chains often dominate the interfacial interactions of intrinsically disordered proteins, however, backbone contributions are far from negligible. Using a combination of nanoscale force measurements and molecular dynamics simulations, we demonstrated with analogous mussel-mimetic adhesive peptides and peptoids 34-residues long that highly divergent adhesive/cohesive outcomes can be achieved on mica surfaces by altering backbone chemistry only. The Phe, Tyr and Dopa peptoid variants used in this study deposited as dehydrated and incompressible films that facilitated analysis of peptoid side chain contributions to adhesion and cohesion. For example, whereas Phe and Dopa peptoids exhibited similar cohesion, Dopa peptoids were ~3 times more adhesive than Phe peptoids on mica. Compared with the peptides, Phe peptoid achieved only ~20% of Phe-peptide adhesion, but the Dopa peptoids were >2-fold more adhesive than the Dopa peptides. Cation- $\pi$ interactions accounted for some but not all of the cohesive interactions. Our results were corroborated by molecular dynamics simulations and highlight the importance of backbone chemistry and the potential of peptoids or peptoid/peptide hybrids as wet adhesives and primers.

18

19 20

21

22

23

24

#### I. INTRODUCTION

Marine mussels produce a tough byssus to adhere to rocky substrates in habitats along turbulent wind- and wave-swept seashores<sup>1</sup>. Biochemical and molecular analysis of byssal adhesive plaques has shown that mussel foot peptides and/or proteins (Mfps) particularly rich in two amino acids, 3,4-dihydroxyphenylalanine (Dopa) and lysine (Lys) are commonly localized

at the interface between each plaque and the underlying substratum<sup>1,2</sup>. The catecholic and cationic side-chains of these residues work separately and in synergy to maximize both adhesion and cohesion. We define adhesion as bonding between the adhesive polymer and the underlying surface, whereas cohesion refers to bonds within the adhesive. Adhesion and cohesion can result from many interactions, including charge-charge interactions between Lys and negative surface charges, mono- and bi-dentate hydrogen bonding between Dopa and surface oxides, metal chelation between Dopa and surface transition metals, cation- $\pi$  bonding between Lys and aromatic side chains, oxidative coupling between Dopa and other residues, hydrophobic interactions, and  $\pi$ - $\pi$  coupling<sup>1,3-5</sup>. Although numerous studies have shown that native adhesive proteins display diverse adhesive/cohesive interactions on various polymer, mineral and oxide surfaces, 4,6-14 the desire for simple mechanistic insights has driven the design and testing of adhesive analogs of reduced complexity. In this way, mussel-inspired peptides and other small molecules have been utilized to investigate the relative importance of each of the above-listed intermolecular interactions. Largely absent has been an exploration of contributions by peptide backbone chemistry and structure to intermolecular adhesive forces. Although the peptide sequences relevant to the mussel system are intrinsically disordered<sup>15</sup>, the peptide backbone inherently influences intra- and intermolecular interactions, enabling transient β-sheet-like structures, restricting backbone conformational freedom, and allowing backbone H-bonding to appropriate amino acid side chains.

1

2

3

4

5

6

7

8

9

10

11

12

13

14

15

16

17

18

19

20

21

22

Our study was prompted by a previous report <sup>16</sup> that concluded counterintuitively that the adhesive performance of mussel foot peptide (Mfp) mimics was largely due to cohesive effects. The authors used an Mfp-5-derived sequence that was adjusted to 3 increasing steps in

aromatic ring hydroxylation (Fig. 1) and measured the adhesion forces required to separate atomically smooth mica surfaces coated with these molecules under acidic pH (~3) and high ionic strength (> 250 mM) regimes. Peptides containing phenylalanine (Phe), tyrosine (Tyr), or 3,4-dihydroxyphenylalanine (Dopa) (Fig. 1B) consistently adsorbed as multilayer films and all forces measured were cohesive. Surprisingly, the Phe-peptides exhibited the strongest cohesive interactions. The Tyr- and Dopa-containing homologs though similar in performance, achieved only a third of the Phe cohesion. Based on these results as well as solution NMR of the peptides, they concluded that cation- $\pi$  interactions are largely responsible for cohesion, and that cohesion is reduced in the cases of Tyr and Dopa by entropically unfavorable steric contributions of hydroxyl groups. In this report, we explore the role of backbone chemistry and structure in the adhesive/cohesive interactions of the mussel adhesive mimetic sequences. Accordingly, we synthesized peptoid analogs (Fig. 1A) of the previously studied peptides and measured their surface interactions with mica using the surface forces apparatus (SFA) (Fig. 1C).

Peptoids differ from peptides by relocating the side chains from the  $\alpha$ -carbon to the amide nitrogen (Fig. 1A, B). This change leads to an achiral  $\alpha$ -carbon, removes amide hydrogens (and therefore the potential for backbone hydrogen bond donation), and weakens the electron delocalization in the polyamide backbone bonds, giving the backbone more conformational freedom<sup>17,18</sup>. The lack of an amide hydrogen bond donor in peptoids prohibits the formation of backbone-stabilized secondary structures such as  $\alpha$ -helices and  $\beta$ -sheets. We observed differences between the adhesion/cohesion strengths of asymmetrically- and symmetrically-deposited peptoid films resulting from the

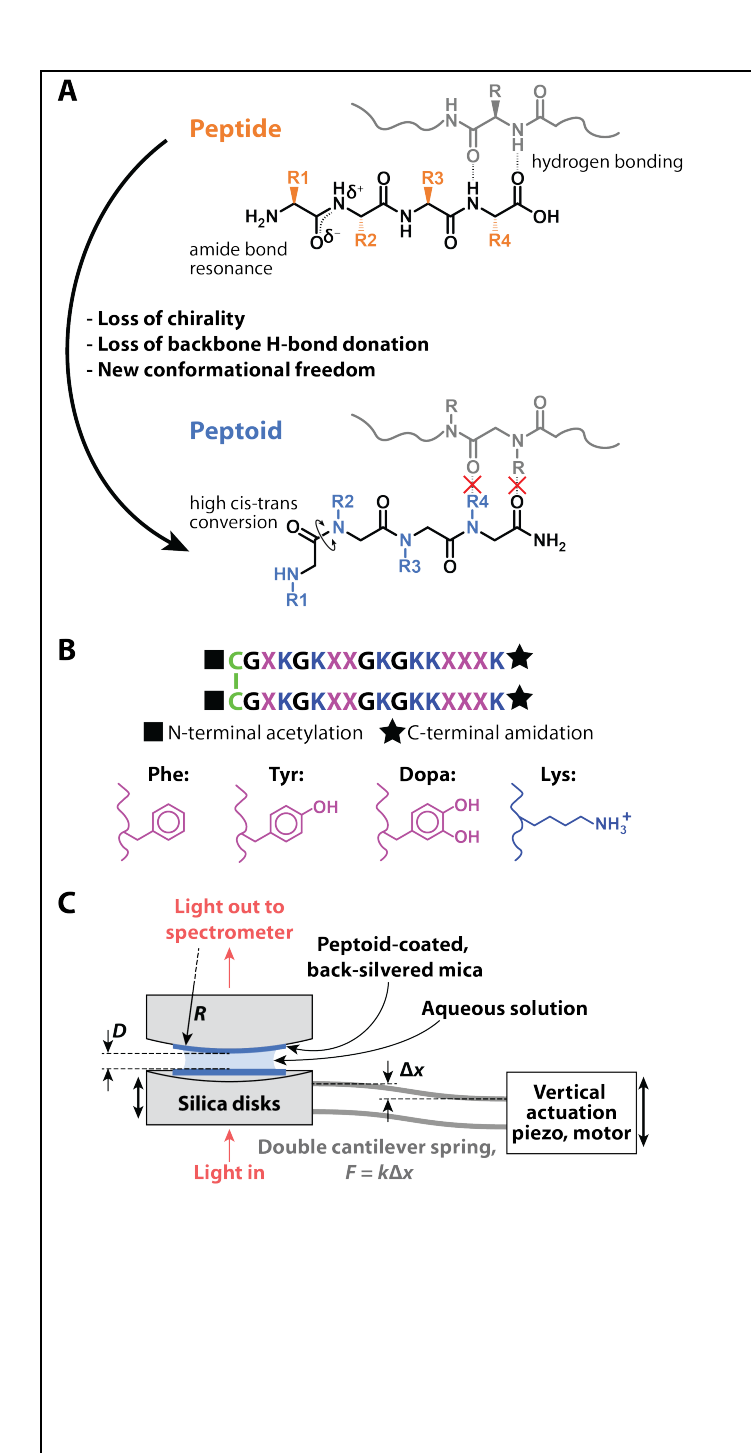


**Figure 1.** – Chemistry and experimental chemical description illustrating the differences between generic peptide (top) and peptoid (bottom) molecules. B) The sequence relevant to all peptides and peptoids discussed in this manuscript. For each molecule, the "X" position in the sequence can be either Phe, Tyr, or Dopa (purple) is internally and consistent for each molecule tested. A cystine linkage, used to double the peptoid molecular weight, is depicted by C-C (green). The lysine side chain is depicted in blue and the glycine side chain (G) is simply -H. C) Schematic of the SFA 2000 used to measure force vs. distance profiles and adhesion/cohesion forces in this study.

- absence of backbone hydrogen bonding groups. Our SFA results indicate peptoid films are less hydrated which we attribute to the increased backbone hydrophobicity. These results are
- 3 corroborated with molecular dynamics (MD) simulations of both the peptide and peptoid
- 4 molecules in solution and at mica surfaces.

#### II. Experimental and Simulation Methods:

#### Materials:

1

2

3

4

5

6

7

8

9

10

11

12

13

14

15

16

17

18

19

20

21

22

Triethylamine (TEA), methyl trifluoroacetate (MeTFA), pyridinium p-toluenesulfonate (PPTS), triisopropylsilane (TIPS), and methanol, potassium nitrate, acetic acid, dimethylformamide (DMF), anhydrous sodium sulfate, mushroom tyrosinase (3,000 U/mg), N-tboc-1,4-diaminobutane, and all FMOC-protected amino acids were purchased from Sigma Aldrich and used as received. Ethyl acetate (EtOAc), tetrahydrofuran (THF), and dichloromethane (DCM) were purchased from VWR. Lithium hydroxide, hydroxybenzylamine, 3,4-dihydro-2H-pyran (DHP), bromoacetic acid, trifluoroacetic acid (TFA), and benzylamine were purchased from ACROS Organics. Diisopropylcarbodiimide (DIC) was purchased from Chem-Impex International, Inc. Rink amide resin was purchased from Novabiochem. All materials and solvents purchased were reagent and HPLC grade, respectively. Peptides used in this study were prepared for previous investigations<sup>12,16</sup>.

#### **Submonomer synthesis:**

Tfa protection of 4-hydroxybenzylamine. 4-hydroxybenzylamine (25 g, 203 mmol) and TEA (85 mL, 609mmol) were added to methanol and stirred for 10 minutes until fully dissolved. MeTFA (52 g, 406mmol) was then slowly added over a period of 20 min, and the reaction mixture was stirred at room temperature overnight. Reaction completion was determined by ninhydrin. The solvent was removed via rotary evaporation. The residue was treated with 1N HCl (100 mL) and extracted with ethyl acetate (3x75 mL). The organic layer was washed with 1N HCl (100 mL), brine (100mL), dried over Na<sub>2</sub>SO<sub>4</sub>, filtered, and the solvent removed to afford a brown solid (40 g, 88%).

THP protection of Tfa-4-hydroxybenzylamine. Tfa-4-hydroxybenzylamine (40 g, 183 mmol) and PPTS (6.28g, 25mmol) were added to a 1000mL round bottom flask and dissolved with DCM (250mL). DHP (42.7g, 507.5 mmol) was added over a 20 min period via an addition funnel. After 1 hour of stirring the reaction mixture at room temperature a white precipitate formed. The reaction was stirred over night at room temperature. The reaction mixture was cooled to -20°C and the white, crystalline precipitate was removed by filtration and washed with cold DCM and dried under high vacuum yielding the product as white crystals (30.6 g, 101 mmol, 55% yield).  $^{1}$ H NMR (400 MHz CHCl<sub>3</sub>):  $\delta$ (ppm) 7.23 (d, J=8.6Hz, 2H), 7.06 (d, J=8.6Hz, 2H), 5.44 (t, J=3.1Hz,1H), 4.47 (d, J=5.9Hz, 2H), 2.00 (m, 1H), 1.87 (m, 2H), 1.66 (m, 3H).

Tfa-deprotection. Lithium hydroxide (2.75g, 57.5 mmol) dissolved in 100mL H<sub>2</sub>O was added to a stirring solution of Tfa/THP protected 4-hydroxybenzylamine (17.5g, 57.7mmol) dissolved in THF (200mL) in a 1000 mL round bottom flask. The reaction was stirred for 3 hours, after which the THF was removed by rotary evaporation. Water (50 mL) was added, and the aqueous solution was extracted with ethyl acetate (3x100mL). The organic layers were combined, washed with water, dried over Na<sub>2</sub>SO<sub>4</sub> and evaporated down to a yellow oil (9.54 g, 80%). H NMR (400 MHz CHCl<sub>3</sub>):  $\delta$ (ppm) 7.2 (d, J=8.6Hz, 2H), 7.01 (d, J=8.6, 2H), 5.39 (t, J=3.1Hz, 1H), 3.89 (m, 1H), 3.77 (s, 2H), 3.58 (m, 1H), 1.99 (m, 1H), 1.84 (m, 2H), 1.63 (m, 3H).

#### Peptoid synthesis:

Peptoids were synthesized using a Symphony X automated peptide synthesizer on a 50  $\mu$ M scale using Rink amide resin (0.64mmol/g). Peptoid coupling was as in previously published procedures<sup>19</sup>. Bromoacetylation was achieved by treatment with DIC (0.8 M in DMF) and

bromoacetic acid (0.8 M in DMF), and displacements by treatment with 1M amine concentration. THP protected 4-hydroxybenzylamine, benzylamine, and N-t-boc-1,4-diaminobutane were used as tyrosine, phenylalanine, and lysine mimics, respectively. Glycine and cysteine were incorporated using standard Fmoc solid-phase synthesis procedures<sup>20</sup>. Couplings were performed using a solution of Fmoc-protected amino acid (0.8 M in DMF) and DIC (0.8 M in DMF) for 20 min. The Fmoc protecting group was removed by treating the resin with a 20% piperidine solution in DMF for 10 min. The N-termini of oligomers were acetylated on resin by treatment with a solution of acetic anhydride (3 parts) and pyridine (2 parts) for 30 minutes. Peptoids were cleaved from the resin by treatment with 95:2.5:2.5 TFA/H<sub>2</sub>O/TIPS for 30 minutes. Solvent was removed from cleaved peptoids using a Biotage V-10 evaporator, and the crude peptoids were dissolved in 5% acetonitrile. Purification was achieved using reverse-phase HPLC with a C18 semipreparative column at a flow rate of 10mL/min.

**Peptoid modification.** Peptoids were dimerized with disulfide linkages as described previously<sup>16</sup>. Monomers (1 mg) were dissolved in 0.1 M phosphate buffer (1mL, pH=7) and NalO<sub>4</sub> was added (10μL, 5mg/mL). The solution was shaken for 20 minutes, filtered, and injected onto a reverse-phase HPLC using a C18 column and purified with a linear gradient of aqueous acetonitrile (5 - 70%). Protein elution was monitored at 280 nm and the peak fractions were analyzed by matrix-assisted laser desorption ionization mass spectrometry (MALDI-MS).

The Tyr peptoid was modified by mushroom tyrosinase to obtain the Dopa peptoid<sup>12</sup>. The peptoid containing the tyrosine mimic (1 mg) was dissolved in a 100mM phosphate/50mM borate buffer (1 mL, pH=7). Mushroom tyrosinase (0.3 mg) was added and the solution

bubbled with oxygen for 4 hours, after which the reaction was stopped by the addition of glacial acetic acid ( $50\mu L$ ). This solution was then filtered, purified by reverse-phase HPLC, and analyzed with MALDI-MS as described for the dimerization process. Fractions containing the most Dopa residues (10-13) were frozen, lyophilized, and resuspended in 100 mM acetic acid (Sigma-Aldrich) buffer (pH = 2.5) to ~1 mg/mL and stored at -80°C°.

6

7

8

9

10

11

12

13

14

15

16

17

18

19

20

21

22

5

1

2

3

4

#### **Surface Forces Apparatus Measurements:**

Standard SFA procedures were used to measure force vs. distance profiles, normalized by the contact radius (F(D)/R) as previously detailed<sup>21</sup>. Before each experiment, the thickness of the mica was measured in air. Subsequently, a peptoid film was established on one (asymmetrical deposition) or both (symmetrical deposition) of the mica surfaces. To deposit a peptoid film, the mica surface was removed from the SFA in a laminar flow cabinet and exposed to 3 mL of 250 mM KNO<sub>3</sub>, 100 mM acetic acid (pH 2.5-2.8) solutions. Subsequently, 15 µL of a 1 mg/mL peptoid solution in 100 mM acetic acid was diluted into the 3 mL salt solution and the surface was incubated for 20-30 min. The surface was then flushed with generous amounts (5-10 mL) of peptoid-free salt solution and transferred back into the SFA, carefully kept wetted by a droplet of solution. Therefore, symmetrical deposition resulted in contact between peptoid films on each surface, while asymmetrical deposition resulted in contact between a peptoid film and a bare mica surface. These experimental conditions were chosen to identically match those used by Gebbie et al<sup>16</sup>. The two surfaces (Figure 1C) were then brought into molecular contact at nm/s velocities, generating the 'Compression' curves of force-distance profiles. After compression, the surfaces were retracted at nm/s velocities following a ~5 min total contact time. During separation, the double cantilever springs (Figure 1C) progressively accumulate tensile stress until the surfaces abruptly jump apart to distances > 500 nm. The jump distance multiplied by the cantilever spring constant, k, measures the force of adhesion (or cohesion),  $F_{\rm ad}$ , between the surfaces. For comparison between experiments,  $F_{\rm ad}$  is normalized by the measured contact radius of the interacting surfaces for each experiment. Because of the mixed adhesive/cohesive failure modes in these systems,  $F_{\rm ad}$  is not normalized to an adhesion energy by either the Derjaguin approximation<sup>21</sup> or the Johnson-Kendall-Roberts (JKR) theory of adhesion<sup>22</sup>.

### **Molecular Dynamics Simulations**

The simulations were performed using the software GROMACS 2018<sup>23</sup>. The GROMOS 53A6 force field<sup>24</sup> was used for the peptides and a new set of parameters consistent with the GROMOS 53A6 peptide force field was developed for the peptoids (Cunha, K. C.; Shea, J. E.; unpublished data, Supporting Review Only). The mica model consisted of a single layer of *muscovite-2M*<sub>1</sub> (KAl<sub>2</sub>(Si<sub>3</sub>Al)O<sub>10</sub> (OH)<sub>2</sub>)<sup>25</sup> comprised of 5,120 atoms and the INTERFACE force field parameters used for the surface<sup>26</sup>. Atomic point charges for the catechol hydroxyl groups were estimated by a RESP fitting<sup>27</sup> from calculations using MP2/6-31G\*\* within NWChem 6.1<sup>28</sup>, as described earlier<sup>29</sup>. After solvation, the energy was optimized using up to 100,000 steps of the steepest descent algorithm.

**Simulations in bulk water**: The starting structure for the molecular dynamics simulations consisted of the peptoid/peptide molecules in SPC water molecules model<sup>30</sup> with 12 Cl<sup>-</sup> ions for neutral charge. The initial systems consisted of the extended peptoid/peptide structures in a cubic simulation box (10x10x10 nm). After 20 ns of simulation, the final (and

more compact) structure was placed into a smaller box (6x6x6 nm) to run for 1 µs. Periodic boundary conditions were used in the x, y and z axes with the NPT ensemble. The LINCS method<sup>31</sup> was used to constrain bonds involving all atoms. The Leapfrog algorithm<sup>32</sup> was used with a time step of 2-fs. Long-range electrostatic interactions were treated using the PME method<sup>33</sup> and short-range electrostatics and van der Waals interactions were computed within the cutoff radii of 1.2 nm and updated every 10 steps with the cut-off scheme Verlet. The temperature was kept at 300 K using the Nose-Hoover scheme<sup>34</sup> and 0.5 ps as a time constant for coupling, using the isothermal compressibility of 4.5  $10^{-5}$  bar<sup>-1</sup>. Two groups were used to couple temperature separately: one containing the peptide/peptoid and another one with the remaining atoms. The Parrinello-Rahman barostat<sup>35,36</sup> was used to couple pressure at 1 bar isotropically with a time constant of 2.0 ps. The center of mass motion was removed at every 100 steps. Other variables were kept at their default values in the Gromacs package.

The last frame of the 1 µs simulation was used as the initial frame of the REMD simulation, which consisted of 64 replicas. Initially, each replica was heated in NVT simulations for 5 ns using the v-rescale scheme<sup>34</sup> with a relaxation time of 0.1 ps. A temperature range of 294 to 500 K was used, with on average an exchange rate between adjacent replicas of 25%, calculated at the initial 10 ns of simulation. The exchanges between replicas were attempted every 3 ps. The REMD simulations were performed for 500 ns at NVT, using the Nose-Hoover scheme<sup>34</sup> and 1 ps as a time constant. A cut-off of 1 nm was used for the short-range electrostatics and the *pair list* update was automatically set to 100 steps. The center of mass motion was removed at every 500 steps.

Simulations on mica: The structure obtained from the 1 μs simulation of each peptoid/peptide molecule in bulk water was used as the starting structure in these REMD simulations. The structures were placed at a minimum distance of about 1.5 nm away from mica. The systems were solvated with SPC water model molecules<sup>30</sup> with 244 K<sup>+</sup> ions in a box size of 8.71108x7.56629x8.00000. Initially, the systems were slowly heated to 300 K in NVT simulations for 1 ns, using the v-rescale scheme<sup>34</sup> with a relaxation time of 0.1 ps. Followed by a second equilibration to have each of the 80 replicas of the systems at a temperature ranging from about 295 to 470 K. The temperatures were chosen to have an average exchange rate of 25% between adjacent replicas, calculated during 1 ns of simulation. The exchanges between replicas were attempted every 3 ps. The REMD simulations were performed for 500 ns at NVT. During all those simulations the mica atoms (except hydrogen) were held stationary. Other conditions for these REMD simulations are the same as described for the REMD simulations in bulk water.

**Simulation Analysis**: The GROMACS tools g\_mindist, g\_hbond, g\_pairdist, g\_gyration, and g\_cluster were used to measure the number of contacts between Lys and mica; hydrogen bonding; the backbone maximum distances (R<sub>max</sub>); the radius of gyration (R<sub>g</sub>) and to cluster the structures of peptides/peptoids. The clusters criteria were: RMSD cutoff of 1.4 Å for the backbone atoms (excluding the tip residues), using the algorithm described by Daura et al.<sup>37</sup> Hydrogen bonds cutoffs were: 3.5 Å for the distance Donor – Acceptor and 30° for the angle Hydrogen - Donor - Acceptor. The secondary structure contents were calculated by DSSP.<sup>38,39</sup> Molecular representations were generated by Visual Molecular Dynamics (VMD) 1.9.4.<sup>40</sup>

#### Circular Dichroism

CD spectra were collected on a JASCO J-1500 circular dichroism spectrometer at 25°C with a scan range of 200-250 nm, scan speed of 20 nm/min, digital integration time of 8s, and with 3 scans being averaged. Solutions of Phe and Tyr-peptide dimers were prepared at a concentration of 20µM in 10mM AcOH and experiments were run using a 0.5 mm pathlength quartz cuvette. To estimate secondary structure content the peptide spectra were decomposed using the BeStSel algorithm<sup>41</sup>.

#### III. RESULTS

#### Peptoid Design

To facilitate comparison with the peptides reported by Gebbie *et al.*,  $^{16}$ , we synthesized matching peptoids for the distinctive adhesive sequence *i.e.* GYKGKYYGKGKKYYYK (res# 30-45 in mfp-5<sup>42</sup>) with one Cys added at the N-terminus for peptide coupling. Each peptoid sequence consists of the peptoid analogs for the amino acids lysine (Lys), glycine (Gly), and counterparts to each of phenylalanine (Phe), tyrosine (Tyr) or 3,4-dihydroxyphenylalanine (Dopa). The Cys-S-S-Cys linkage served to lengthen the construct as in the previous peptide study<sup>16</sup>. The locations and quantities of the Gly, Cys, Lys, and aromatic amino acids are conserved among the three peptoids (Fig. 1B). The high charge content of the peptoid sequences, afforded by a ~35 mol% Lys composition, allows these molecules to displace hydrated K<sup>+</sup> on mica surfaces<sup>43</sup> and form multiple coulombic surface interactions per peptoid molecule, thereby bonding them to the mica surface. The aromatic side chains (Phe, Tyr, Dopa) were included to mediate other interactions such as hydrophobic interactions, cation- $\pi$  complexation,  $\pi$ - $\pi$  interactions, and hydrogen bonding (in the case of Tyr and Dopa).

## Results with the surface forces apparatus (SFA)

Mica surfaces, such as those schematically depicted in Fig. 1C, are minimally adhesive  $(F_{ad}/R < 2 \text{ mN/m}, \text{Fig. 2})$  when exposed to the 250mM KNO<sub>3</sub>, 100mM acetic acid solutions used in this study (high salt conditions), and separated at several nm/s. The separation force increased after deposition of each Phe, Tyr, or Dopa peptoid variant. The blue bars in Figure 2 show the separation forces mediated by each peptoid. Solid bars correspond to peptoids deposited asymmetrically onto one mica surface only (Fig. 2, inset, left), whereas

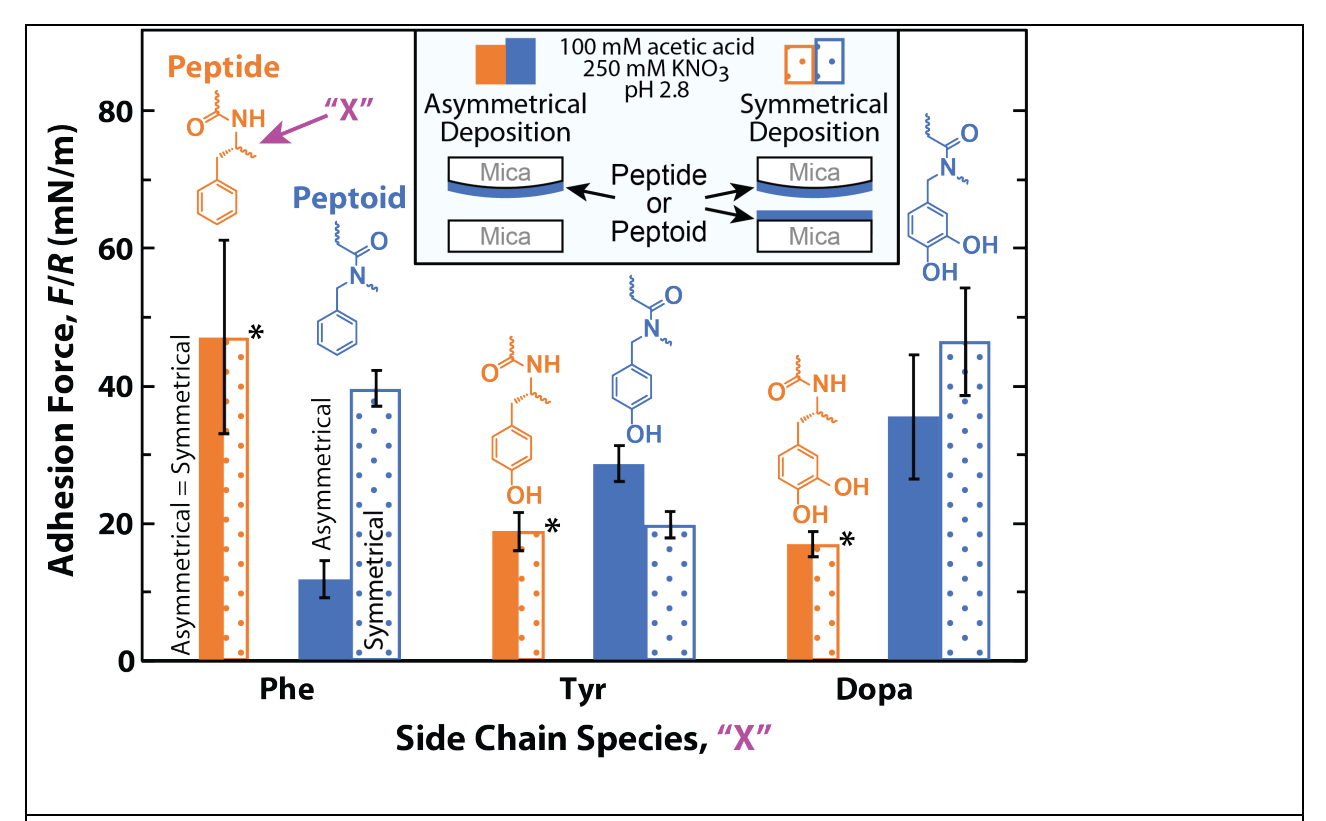


**Figure 2.** Adhesive and cohesive interactions. Adhesive and cohesive forces between asymmetric (*solid bars*) and symmetric (dotted bars) films on mica surfaces in the SFA comparing peptide (orange) and peptoid (blue) films. Error bars denote means with standard deviations. Inset shows test configurations with the background solution conditions. The aromatic residue present in each peptide/peptoid variant is

illustrated above each set of bars. To allow for comparison between datasets, the peptoid experiments were conducted under conditions identical to those of the previous peptide experiments. \*Adapted in part with permission from Gebbie *et al.*<sup>16</sup>

dotted bars correspond to peptoids deposited symmetrically onto both mica surfaces (Fig. 2, inset, right). The Dopa peptoid separation force did not depend on the deposition method, that is, asymmetric and symmetric deposition of the Dopa peptoid resulted in the same separation force. However, the forces mediated by the Phe and Tyr peptoids did depend on deposition symmetry: a film of Phe peptoid deposited asymmetrically mediated lower separation force than films of Phe peptoid deposited symmetrically, and a film of Tyr peptoid deposited asymmetrically mediated a larger separation force than symmetric Tyr peptoid films.

By comparison, the orange bars in Figure 2 show separation forces mediated by the peptide analogs studied by Gebbie *et al.*<sup>16</sup> Because these peptides never deposit as monomolecular films the separation forces did not depend on the deposition method. Each bar is shown as both solid and dotted to indicate that asymmetric or symmetric depositions had the same outcome.

Overall, the range of observed peptoid forces is similar to the reported peptide forces. However, whereas measured separation forces (F) in the peptides <u>decreased</u> with increasing hydroxylation i.e.  $F_{Phe} > F_{Tyr} > F_{Dopa}$ , in the asymmetric peptoid films, the opposite trend occurred:  $F_{Phe}, < F_{Tyr} < F_{Dopa}$ . In particular, the separation force measured for the asymmetrically deposited Phe peptoid was only ~25% of measured Phe-peptide force, whereas the Dopa peptoids were at least two-fold more adhesive than the Dopa peptides.

Peptoids deposited symmetrically showed a different trend: Phe peptoid separation forces did not differ significantly from those of the Phe peptide. Similarly, the separation force

measured for the Tyr peptoid was not significantly different from the force measured for the

Tyr peptide. However, symmetric Dopa peptoid films >2-fold higher separation forces than the

corresponding Dopa peptide.

In addition to the values for the adhesive/cohesive forces, the force vs. distance profiles (F(D)/R) revealed that the peptoids adsorbed as minimally compressible films. Because our deposition technique (see Methods section) required removal of mica surfaces from the SFA, a specific film thickness at maximal compression (a film's hard wall) was not measurable. However, the relative behavior of the films while under compression was quite accurate. Representative compression runs for each peptoid are depicted in Figure 3A and the curves are shifted along the abscissa for clearer comparison of their shapes and profiles. The slopes for the three peptoids are nearly identical and are uniformly steeper than either those of the peptoid-free salt solution (Supp. Fig. S1) or those measured for the peptide films (Supp. Fig. S2), which were found to be diffuse and hydrated multilayers 16. This suggests that the peptoids form more compact and less hydrated films than

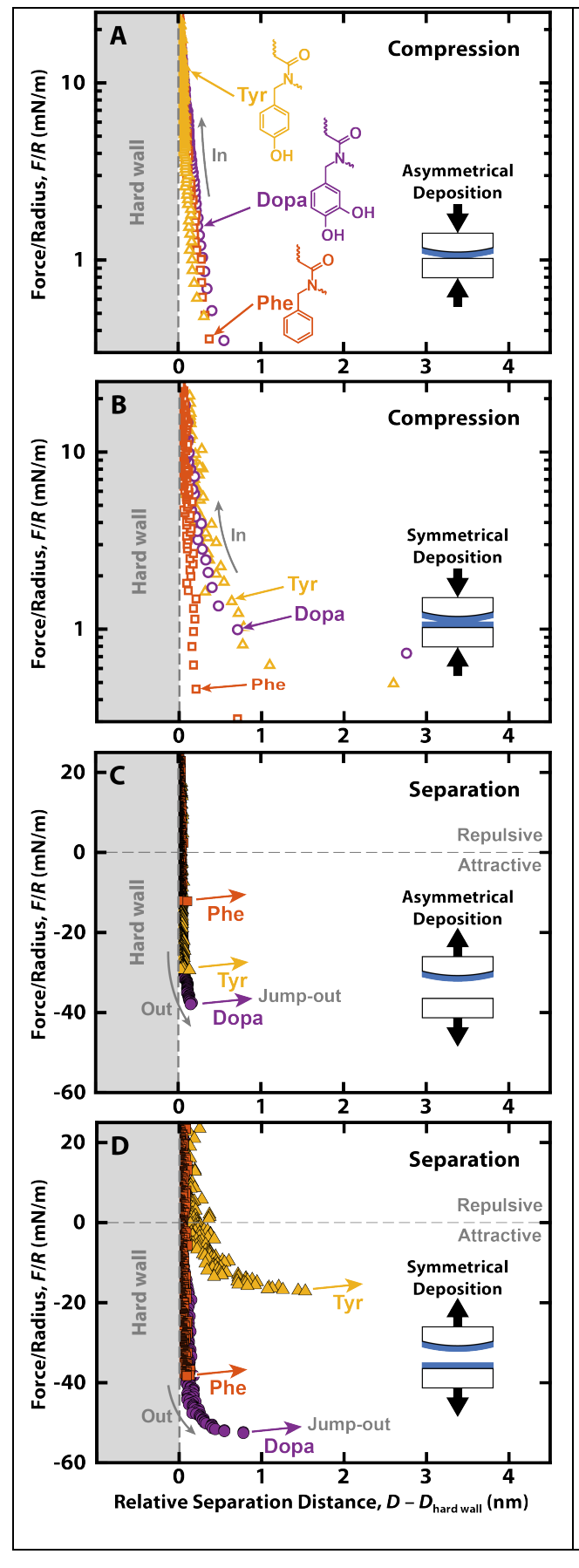


**Figure 3.** Representative force curves for the peptoid molecules reveal low compressibility and low hydration.

Force versus distance profiles for Phe, Tyr, and Dopa peptoids were deposited both asymmetrically (A,C)and symmetrically (B,D)between mica surfaces. Absolute peptoid film thicknesses, Dhard wall, cannot be therefore accurately calculated, relative distances, D - Dhard wall, near maximum compression, provide meaningful alternative comparisons. The compression curves (A, B) are represented with a log scale on the ordinate exponential highlight features axis reminiscent of double-layer and hydration decay lengths.

perhaps because more peptoid material was deposited. Representative separation/decompression runs for the same molecules are shown in Figure 3C-D. The separation curves show small amounts of bridging between the surfaces before separation, commonly observed for polymeric molecules.

# Effect of ionic strength on Dopa peptoid adhesion

The surface and molecular binding properties of Dopa-containing peptides are greatly influenced by the H-bonding and cation- $\pi$  tendencies of Dopa. By extension, similar tendencies are expected for peptoids but need to be tested. By exposing symmetric Dopa peptoid films in the SFA to solutions of constant pH with increasing ionic strength, we controlled electrostatic screening. If the Dopa peptoids failed cohesively at high ionic strengths, then cohesive forces would likely be cation- $\pi$  interactions, which, consistent with other coulombic forces, depend on ionic strength. He gives 4 shows the dependence of Dopa peptoid adhesion force on ionic

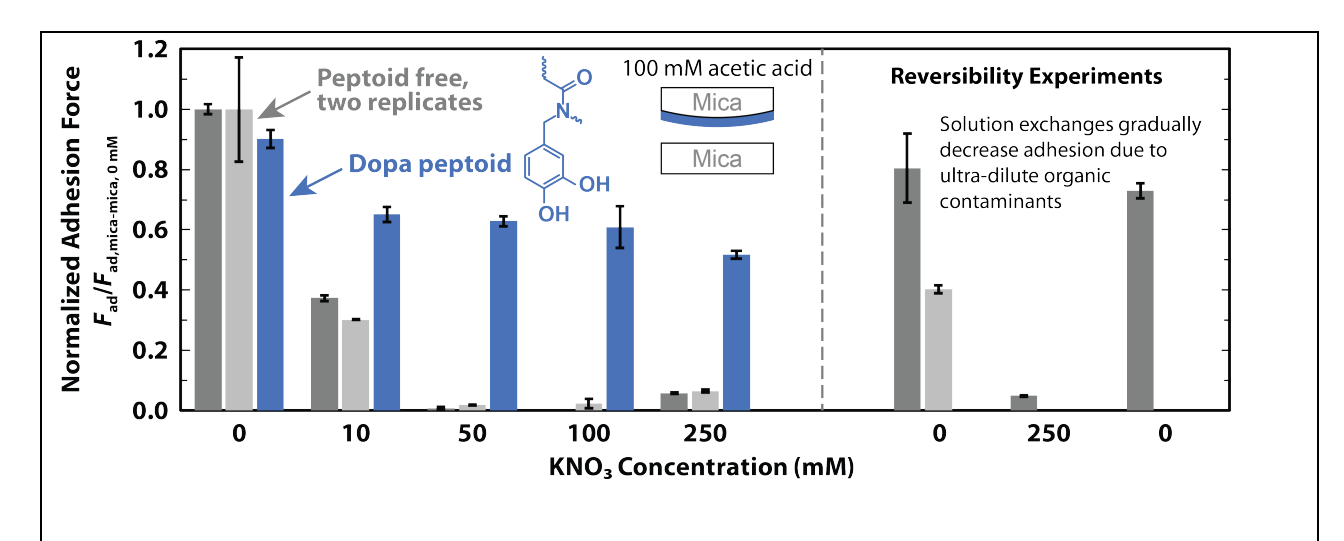


**Figure 4.** Effect of ionic strength on Dopa peptoid adhesion. Adhesion forces for asymmetrically deposited Dopa peptoid films in 100 mM acetic acid and 0, 10, 50, 100, and 250 mM KN0<sub>3</sub> (blue bars) compared with the adhesion forces for peptoid-free mica surfaces (two replicates at the

same conditions are represented by two separate sets of light and dark gray bars). Experiments of the same color bars are chronological (l to r), with solution changes between each set of measurements. In each case, the measured  $F_{ad}$  is normalized by the force of adhesion for the bare mica surfaces (before peptoid deposition) in 100 mM acetic acid without KNO<sub>3</sub>. The 'Reversibility Experiments' demonstrate that partial recovery of the KNO<sub>3</sub>-free bare-mica adhesion is possible over multiple cycles between high and low salt conditions.

1

2

3

4

5

6

7

8

9

10

11

12

13

14

15

16

strength. In these experiments, the Dopa peptoid was deposited using a KNO<sub>3</sub>-free solution. The KNO<sub>3</sub> concentration was then incrementally increased by flushing the intervening capillary between the mica surfaces with 3-5 ml of peptoid-free solution to a new KNO<sub>3</sub> concentration and allowed to equilibrate for >30 min. The adhesive strength of the Dopa peptoid at all conditions remained remarkably similar to that of bare mica surfaces in KNO<sub>3</sub>-free solution. Because of this, we also measured the adhesion of bare mica at all salt concentrations. The data are plotted normalized to the bare mica adhesion force without KNO3 to minimize the effect of geometrical differences on adhesion strength between the contact points. The adhesive performance of the Dopa peptoid between mica surfaces decreased more slowly than that of bare mica surfaces, reaching about 50% of its 0 mM KNO<sub>3</sub> value when finally equilibrated to 250 mM KNO<sub>3</sub> (Fig. 4). To rule out surface contamination as the cause of adhesion loss with increasing salt concentration in the bare mica experiments, reversibility was tested for both mica-mica replicates by flushing the surfaces with alternating 0 M and 250 M KNO<sub>3</sub> solutions. The first bare mica replicate (dark gray) showed reproducible adhesion reversibility over two cycles while the second replicate (light gray) only partially recovered the initial 0 M adhesion force.

#### Molecular Dynamics Simulations

1

2

3

4

5

6

7

8

9

10

11

12

13

14

15

16

17

18

19

20

21

22

To gain insight into the adhesion mechanisms, we performed REMD simulations of each paired peptide/peptoid in bulk water and on mica surfaces. Figure 5A shows a snapshot of the most likely conformation adopted by each molecule in bulk water, with the other top 3 structures shown in the supplementary Fig. S3. In each panel, the probability that the molecule adopts a conformation belonging to the most populated cluster is given in the upper left-hand corner. Overall, the most representative structures adopted by either peptides or peptoids leads to the exposure of the Lys residues to solution. Figure 5B shows the distribution of the radius of gyration  $(R_g)$  versus the maximum distance  $(R_{max})$  between any of the backbone atoms. The lower  $R_g$  and  $R_{max}$  observed for peptoids indicates more compact structures. The Phe peptoid adopted structures that attempt to bury hydrophobic phenylalanine rings and expose the Lys residues, while the Dopa peptoid favors the maximum exposure of Dopa and Lys residues, leading to the most compact structure of all three peptoid variants (Fig. 5B). Peptoids are primarily random-coils, whereas the peptides showed some regions of stable  $\beta$ -sheets (Fig. 5A and supp. Fig. S4 and S5) and present higher values for  $R_{\rm g}$  and  $R_{\rm max}$  as a consequence of forming  $\beta$ -sheets. We performed CD spectroscopy on the Phe and Tyr peptides to investigate their secondary structure (Supp. Fig. S6 and S7). The spectra for Phe and Tyr showed positive ellipticity at 220 and 230 nm, respectively, and the ellipticity became negative at lower wavelengths. The solution spectra are consistent with right-hand twisted  $\beta$ -sheets<sup>41</sup>. The secondary structure prediction of each peptide generated by the BeStSel algorithm indicates both peptides have significant antiparallel β-sheet content (Supp. Table S8) which agrees with our simulations (Fig. 5A, 5B).

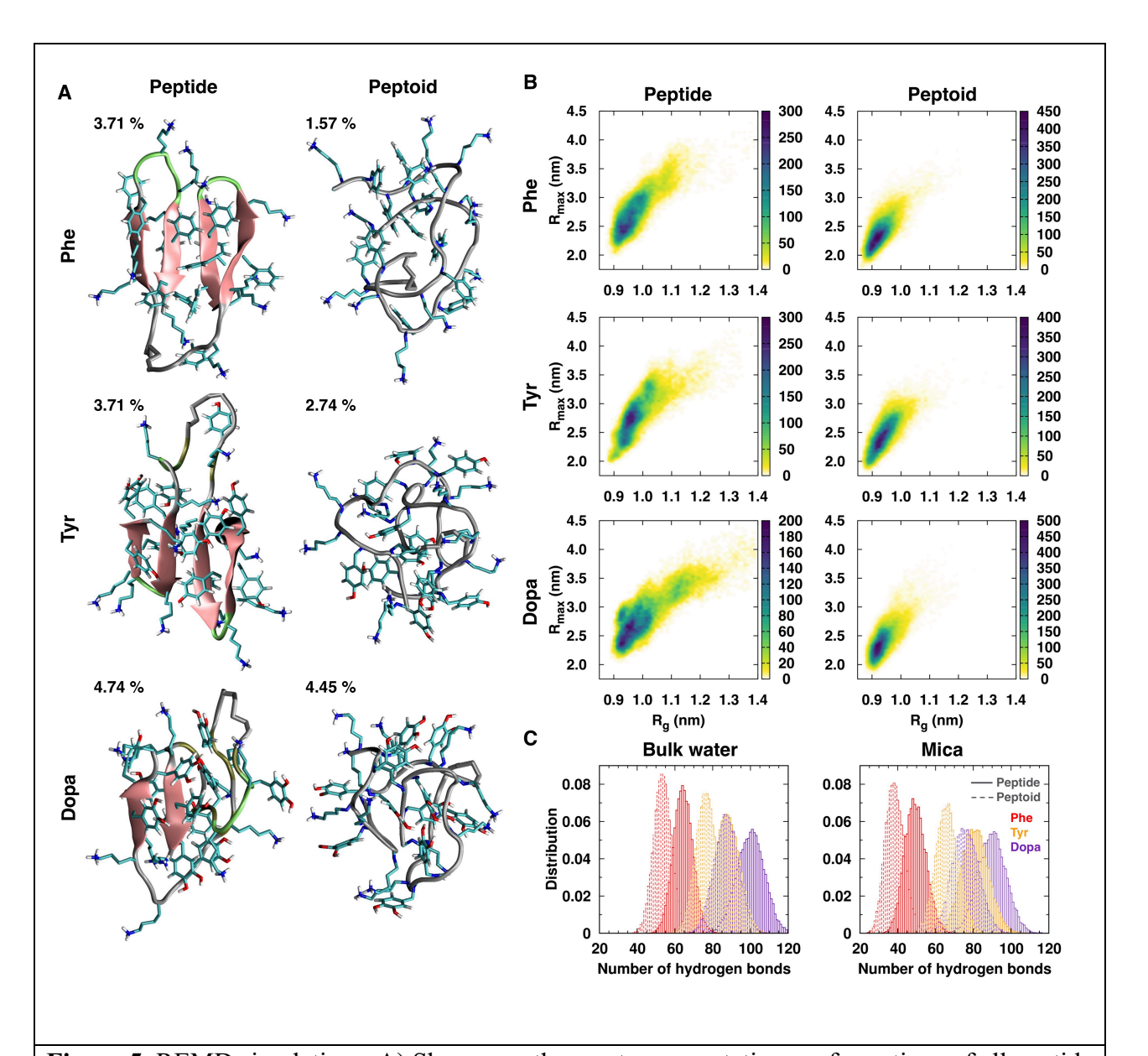


**Figure 5.** REMD simulations. A) Shown are the most representative conformations of all peptide and peptoid homologues in bulk water. The percentage of structures present in the most populated cluster are shown in the *top left*. (a total of 15,000 structures were analyzed). The secondary structure is shown (pink) with β-sheet formation indicated by wide arrows pointing from the N- to C-terminal. β-sheet formation is seen only in the peptide backbones. Atoms are color coded as N: blue; H: white; C: cyan; O: red. B) 2D Distribution of the radius of gyration vs. the maximum distance measured within any backbone atoms. C) Normalized histogram of

the number of hydrogen bonds in between the water molecules and the peptides/peptoids in bulk water (left) and on mica (right). All analyses were done for every 20 ps for the last 300 ns of simulations.

The Phe and Tyr peptoid homologs presented smaller probabilities for the most representative clusters, as well as higher numbers of clusters of likely conformations (Supp. Table S9), indicating that these peptoids sampled a much larger conformational space and had their structures more broadly distributed among their clusters than did the peptides. Although the peptide backbones have a higher number of hydrogen bonds, given the prevalence of secondary amines in peptoids (supp. Fig. S4; S5 and Fig. 6C), the Dopa peptoid showed a number of clusters and the probability for its most representative cluster was comparable with the ones observed for peptides (Fig. 5A and supp. Table. S9). This is likely due to hydrophobic interactions within the backbone and the heightened exposure of Dopa and Lys to the solvent. We also examined peptoid vs peptide hydration in solution and found each peptoid to be less hydrated than its peptide counterpart (Fig. 5C).

To provide insight into the molecular scale forces driving adsorption we modeled the structure of the peptides and peptoids in the presence of a mica surface and monitored the number of phenolic and Lys side-chains in close proximity with the surface. We found that more Lys residues were recruited to the surface than phenolic groups (Fig. 6A, B and Supp. Fig. S10). A snapshot of the most likely conformation adopted by each molecule is shown in Fig. 6A, and the other top 3 structures are shown in supplementary Fig. S11. The probability that the molecule will adopt a conformation belonging to the most populated cluster is listed in the upper left-hand corner of Fig. 6A. Compared with the simulations without mica, the lower

number of total clusters (Supp. Table S9) and the higher probabilities of the most stable cluster in each simulation, indicate that the bound structures are more stable than in bulk water. Fig. 6B shows the distributions of the number of Lys recruited to the surface and radius of gyration along the z-axis, which reflects the spread over the surface plane (x-y plane). The Dopa peptide recruited the lowest number of Lys residues to the surface and also presented the lowest values for  $R_{\rm g(z)}$ . The Dopa peptide also had low  $R_{\rm g}$  and  $R_{\rm max}$  (Supp. Fig. S12), indicating that an individual Dopa peptide adopts compact conformations on mica. This behavior, as well as the lower interaction with the surface as reflected by fewer peptide-surface interactions can be explained in terms of the peptide's higher intramolecular hydrogen bonding (Fig. 6C) and hydrophilicity. On the other hand, the Phe and Tyr peptides and Dopa peptoid showed good surface spreading ability with roughly 11 Lys residues attached to mica. The Phe peptoid also showed high Lys binding to the surface, between 10-12 residues, with lower values observed for  $R_{\rm g(z)}$  reflecting its compact structures (also seen by the distribution of  $R_{\rm g}$  vs  $R_{\rm max}$  in Supp. Fig. S12).

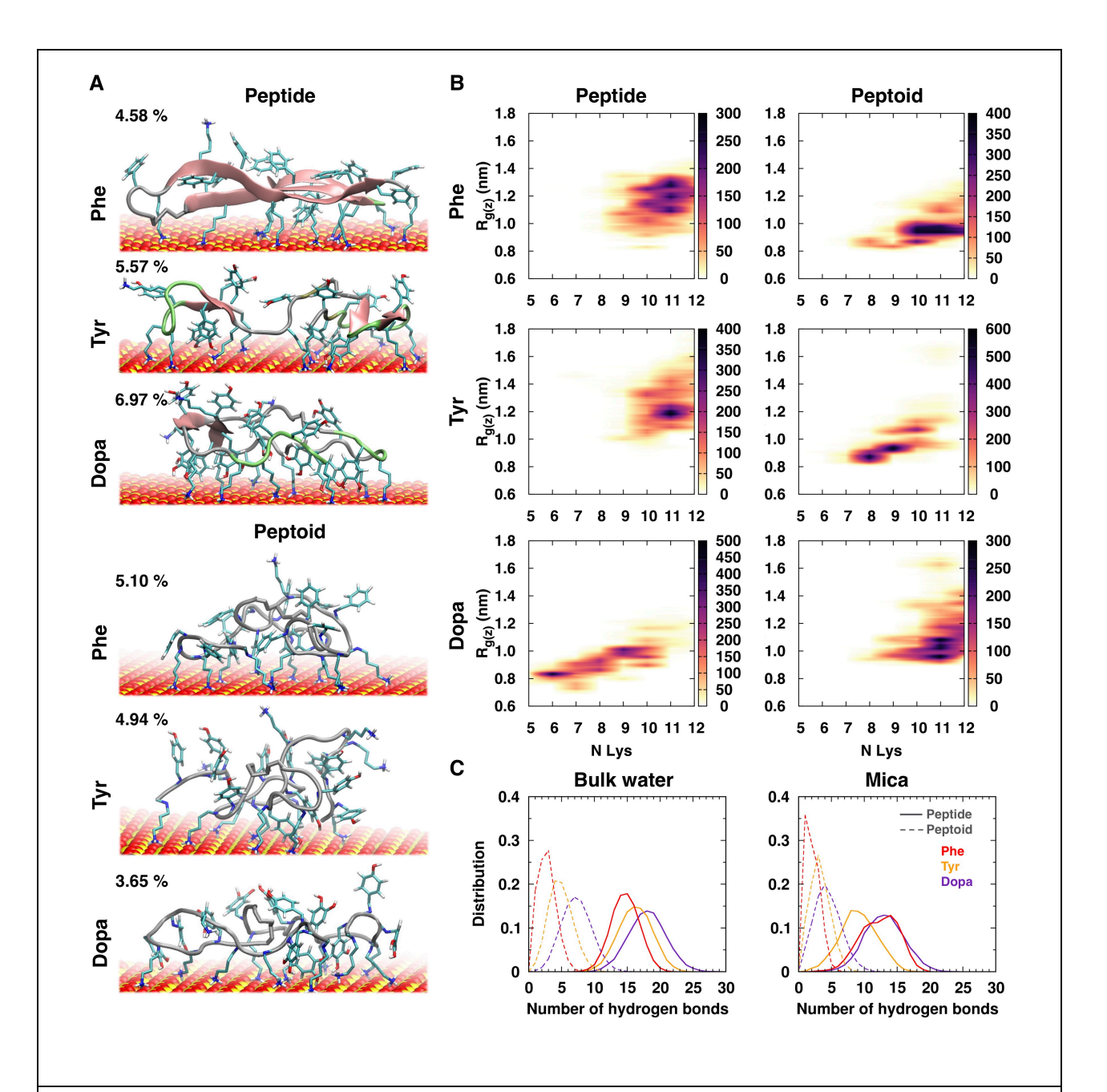


**Figure 6.** REMD simulations. A) Shown are the most representative conformations of all peptide and peptoid homologues in the presence of water. The percentage of structures present in the most populated cluster is shown in the *top left* (a total of 15,000 structures were analyzed). The secondary structure is shown (*pink*) with β-sheet formation indicated by wide arrows having an N- to C-terminal orientation. Atoms are color coded as N: *blue*; H: *white*; C: *cyan*; Si: *yellow*; O:

red; Al: orange. B) 2D Distribution of the number of Lys in close proximity to mica (r < 3 Å) vs. the radius of gyration along z-axis. C) Normalized histogram of the number of intra-molecular hydrogen bonds in bulk water and on mica surface. All analyses were done for every 20 ps for the last 300 ns of simulations.

Following surface adsorption, all molecules showed reduced hydrogen bonding with the solvent (Fig. 5C). Of the adhesive peptides and peptoids considered, the Dopa and Tyr peptides were the most hydrated. Of note is that the secondary structures of Tyr and Dopa peptide unfold most with just a few residues stabilizing  $\beta$ -sheets, whereas the Phe peptides only partially unfold, retaining some secondary structure (Supp. Figures S4; S5).

Considering the results obtained by the SFA experiments, the lower cohesion observed for Dopa peptide is correlated with higher hydration and intramolecular interactions, and its adoption of a compact structure. Similarly, the higher cohesion forces measured for the Pheand Dopa peptoids can be explained in terms of their lower hydration, lack of backbone-mediated intramolecular hydrogen bonds, and their ability to spread over the surface, which exposes the aromatic groups.

Given the complexity of the experimental system with many more molecules, longer time scales, and the myriad of aggregate-forming binding states for peptides/peptoids, we acknowledge that MD simulations have limitations. However, the simulations give us important insights about the mechanisms involved in the adhesion process. Our simulations and experiments concur to the extent that the higher flexibility of peptoids and their inability to form secondary structures provide a barrier against multilayer formation. In addition, the lower

hydration of peptoids and their compact structures is consistent with their relative behavior to
 peptide films.

#### IV. DISCUSSION

Most synthetic mussel-inspired adhesive polymers lack mussel-specific sequences and a polypeptide backbone. A5,46 Consequently, how backbone chemistry impacts adhesion in mussel-inspired systems is rarely investigated. Our results show that even when specific sequences are maintained, subtle changes in backbone chemistry can result in profoundly different adhesive behaviors. We attribute these differences between peptoids and peptides to differences in adsorption. Whereas peptides deposit as multilayers, our results suggest that peptoids deposit on mica surfaces as monomolecular films or nearly so. As a result, asymmetric and symmetric deposition can result in different failure modes and separation forces.

The dependence of the separation forces on the deposition method for Phe and Tyr peptoids gives an indication of the failure mode. The separation force for symmetric Phe was 3-fold greater than for asymmetric Phe, and the separation force for symmetric Tyr was ~2/3 that of asymmetric Tyr. We propose that the changing forces correspond to changing failure modes, namely, asymmetric deposition resulted in adhesive failure, whereas symmetric deposition resulted in cohesive failure. The influence of film symmetry on the failure mode implies that the Phe and Tyr peptoids adsorb as monolayers where a monolayer is defined as a film that is on average one molecule thick. Each of the previously studied peptides deposited as monolayers and failed cohesively, regardless of deposition symmetry<sup>16</sup>. If, like the peptides, peptoids deposited as multilayers, then cohesive failure would be expected after both asymmetrical and

symmetrical deposition. In that case, the separation force measured for the peptoids would also be independent of the deposition method.

That Phe and Tyr peptoids adsorb as monolayers is further supported by the compressibility of the adsorbed peptoid films. The relatively steep slopes of the force-distance curves upon compression are consistent with less hydrated peptoid monolayers adsorbed to mica, in contrast with the previously studied peptides that formed hydrated multilayers (Fig. 3A,B, Fig. S2). Our simulations show that the peptoids have significantly fewer water molecules than the analogous peptides in their first hydration layer (Fig. 5C), consistent with differing levels of hydration between peptoid and peptide films.

Finally, the separation forces for Phe peptoids deposited symmetrically are the same as the Phe peptides. Similarly, Tyr peptoids deposited symmetrically yield the same separation force as the Tyr peptides. These similarities suggest that the functional groups determine the strength of cohesive interactions between the macromolecules and support the assertion that symmetric deposition of Phe and Tyr peptoids results in cohesive failure, like the analogous Phe and Tyr peptides. Given the consistency between the symmetrically deposited Phe and Tyr peptoid with their analogous peptides, the molecular nature of the interactions is assumed to be the same for each class of molecule – namely a combination of hydrophobic interactions, hydrogen bonding (in Tyr species), and a significant contribution of cation- $\pi$  interactions which decay with increasing side-chain ring hydroxylation. Figure 7 depicts a model of these interactions for the Phe and Dopa peptoids.

In contrast with the deposition-dependence of the separation forces for Phe and Tyr peptoids, the separation forces mediated by Dopa peptoids after asymmetric and symmetric

deposition were the same. Furthermore, both symmetric and asymmetric deposition of Dopa peptoids resulted in significantly higher separation forces than the force mediated by the analogous Dopa peptide. We propose two explanation for this behavior. First, adhesive bridging contributes to the performance of the Dopa peptoid films, irrespective of the deposition method. Such adhesive failure, even after symmetric deposition, is possible if the binding functionalities (likely Dopa hydroxyls and lysyl pendant amines) on one surface penetrate the film on the other surface and bind to the underlying mica layer (Fig. 7, bottom right). In that situation, some of the individual peptoid molecules bind to both surfaces, guaranteeing adhesive contributions to the failure mechanism. Similar behavior has been seen previously in a study of small molecules with similar catechol and amine binding functionalities.<sup>47</sup> This scenario is more likely for the Dopa peptoid than either of the other species for two reasons i) the available Dopa-mica binding interactions are more energetically favorable than Phe-mica or Tyr-mica interactions, ii) the REMD simulations demonstrate that Dopa peptoids extend slightly further from the mica surface than Phe and Tyr peptoids (Fig. 6B). An adhesive component of failure strongly suggests that the Dopa peptoid adsorbs as monolayers on the mica surface (Fig. 7, bottom left), since multilayers would present a steric barrier to the formation of bridging interactions. That Dopa peptoids adsorb as monolayers is further supported by the similar compression profiles of Dopa, Tyr, and Phe peptoids in either deposition method.

1

2

3

4

5

6

7

8

9

10

11

12

13

14

15

16

17

18

19

20

21

22

Second, we note that the separation force for Dopa peptoids deposited symmetrically likely includes some contribution from cohesive interactions in addition to adhesive bridging interactions, and that the cohesive interactions are strengthened relative to the Dopa peptide

due to the dehydrated state of the peptoid films. The diminished hydration in Dopa peptoid films means there are fewer water molecules to compete for hydrogen bonding with the catechol moieties. This enables stable bidentate hydrogen bonds to rapidly form between catechol side chains(Fig. 7), which have previously been shown to produce strong cohesive interactions<sup>48,49</sup>. Reduced hydration in combination with the lack of intramolecular hydrogen bonds allowed the Dopa peptoid to better spread over the surface, leaving the side chains more available to form cohesive and adhesive interactions, as observed in our simulations. The proposed ability of the Dopa peptoid monolayers to form both strong bridging adhesive interactions (unlike the peptide multilayers), and strong cohesive interactions due to the peptoid dehydration, are consistent with the greater separation forces measured for peptoids than peptides after both symmetric and asymmetric deposition.

The formation of dehydrated monolayers rather than hydrated multilayers may be understood as follows: The reduced number of interactions between peptoids and water molecules through hydrogen bonds (Fig. 5C) is expected because removal of the amide hydrogen results in a more hydrophobic backbone that also lacks intramolecular hydrogen bonding. Additionally, increased conformational freedom allows peptoids to adopt more compact structures having collapsed backbones. We found that Phe peptide adopts  $\beta$ -sheet conformations both in solution and when presented with a mica surface that may contribute to multilayer formation<sup>50,51</sup>. Phe and Tyr peptides spread over the mica surface and orient most of their aromatic rings upward, which could favor the stacking of molecules. In addition, the larger number of conformational clusters generated by the peptoids on mica is evidence of their flexibility and disorder, which in turn obstructs the formation of diffuse, hydrated, multilayers.

The dependence of the separation force mediated by the Dopa peptoid on the solution ionic strength also provides information about the relative magnitudes of interactions responsible for adhesion. At the highest salt concentration tested (250 mM KNO<sub>3</sub>), forces due to coulombic interactions are expected to be significantly reduced. Possible adhesive interactions include Dopa hydrogen bonding to the mica surface, complexation of aluminum atoms in the mica lattice by Dopa, and Lys-mica bridging, of which only the Lys-mica interactions would depend strongly on ionic strength. Previous results from MD simulations showed that bi-dentate interaction between Dopa residue and mica is a strong interaction that persists throughout the simulation and presents an average length comparable to a coordination bond length, leading to a hydrogen bond lifetime about 20 times higher than the one observed for the Dopa-surface interaction mediated by water molecules or Lys residues (more information in Supp Fig. S13). Possible cohesive forces include cation- $\pi$  interactions, hydrophobic interactions, quadrupole interactions, and Dopa-Dopa hydrogen bonding between the peptoid films. Covalent adhesive and cohesive interactions like oxidative quinone coupling and Dopa coordination bonding can be ruled out based on the reversible separation forces measured in our experiments. Because increasing ionic strength reduced the separation force by up to half (Fig. 4), we conclude that non-Coulombic interactions contribute to approximately half the separation forces, consistent with earlier reports asserting the importance of electrostatic interactions<sup>12</sup> and Dopa-mediated bidentate H-bonds<sup>52</sup> for adhesion of mussel proteins.

1

2

3

4

5

6

7

8

9

10

11

12

13

14

15

16

17

18

19

20

21

22

These conclusions about the adsorption behaviors, failure modes, and likely interactions for films of peptoids and peptides account for the trends in separation forces presented in Figure 2.

We find that for peptoids deposited asymmetrically, the separation force increases with increasing ring hydroxylation from Phe to Tyr to Dopa, consistent with the contribution of hydrogen bonds generating adhesive and cohesive interactions. In the case of the Phe peptoid with the most Lys committed to binding the first surface, an asymmetric Phe peptoid film presents a hydrophobic, Phe-rich face to the second mica surface and forms few hydrogen bonds, resulting in weak adhesion (Fig. 6A). Asymmetrically deposited Tyr and Dopa peptoids mediate greater adhesion due to the ability of the Tyr and Dopa sidechains to form hydrogen bonds, as well as the greater number of unbound Lys available to bind to the other mica surface (Fig. 6C). The Dopa substituted peptoid yielded strong separation forces for both symmetric and asymmetric deposition due to a combination of adhesive bridging interactions and enhanced cohesion due to dehydration.

In contrast, Gebbie *et al.* found decreasing separation force with increasing ring hydroxylation, but the separation forces reported in that work corresponded to cohesive failure rather than adhesive failure, and are consistent with the cohesive forces measured here for symmetrically deposited Phe and Tyr peptoids. The relatively strong cohesion of the Phe macromolecules likely resulted from the geometry: with Lys down on mica and Phe up toward solvent in films on both surfaces, the peptoid and peptide films cohere via hydrophobic interactions and  $\pi$ - $\pi$  coupling between phenyl groups, and cation- $\pi$  bonding between phenyl groups and lysine groups not bound to the mica surface. The hydroxyl group in the Tyr peptoid and peptide is expected to lower the strength of hydrophobic and cation- $\pi$  interactions<sup>16</sup>. Finally, the multilayers of the Dopa peptide inhibit bridging adhesion and the presence of water interferes with the formation of stronger interactions as discussed above.

It is not surprising that the incorporation of Dopa into different polymer systems may produce variable results. Mfp-5 is a surface primer whose sequence is rich in Dopa (up to 30mol%)<sup>1</sup>, and proteins such as this have inspired numerous synthetic catechol-functionalized adhesive polymers. The synthetic systems have met with variable success in part because they may not recapitulate the context or conditions present in the mussel plaque. Dopa is a reactive side-chain in vitro but in the adhesive plaques Dopa redox is maintained regardless of the ambient solution conditions.<sup>53</sup> The protein cohort forming the adhesive plaque is deposited as a coacervate phase at low pH <5.9 Protein coacervates resemble peptoids in that during liquidliquid phase separation both release significant H<sub>2</sub>O.<sup>54</sup> This is also consistent with work suggesting that Dopa residues in Mfp-3 variants are shielded from the aqueous phase by being nested in a hydrophobic environment.<sup>55</sup> In a similar fashion, the peptoids used in this study, unlike their peptide counterparts, deposit with a lower degree of hydration and consequently enable strong Dopa-mediated adhesion and cohesion despite having the same sequence of functional groups and an analogous polyamide backbone. It must be emphasized that mica was the only substrate used in this study and that the basic region of mfp-5 (characterized by high Dopa, Lysine, and Glycine) was the only sequence tested. Other domains in mfp-5 have different charge characteristics with lower adhesion on mica<sup>12</sup>.

1

2

3

4

5

6

7

8

9

10

11

12

13

14

15

16

17

18

19

20

21

22

The peptoids used in this study showed very different adsorption behavior from their peptide counterparts, and a different balance of adhesion and cohesion, despite having the same sequence of functional groups and an analogous polyamide backbone. These results demonstrate that small changes in backbone structure and hydration influence molecular conformations, adsorption, and ultimately adhesive function, and provide insight into the

1	design rules and processing conditions for optimizing the performance of mussel-inspired
2	adhesives.

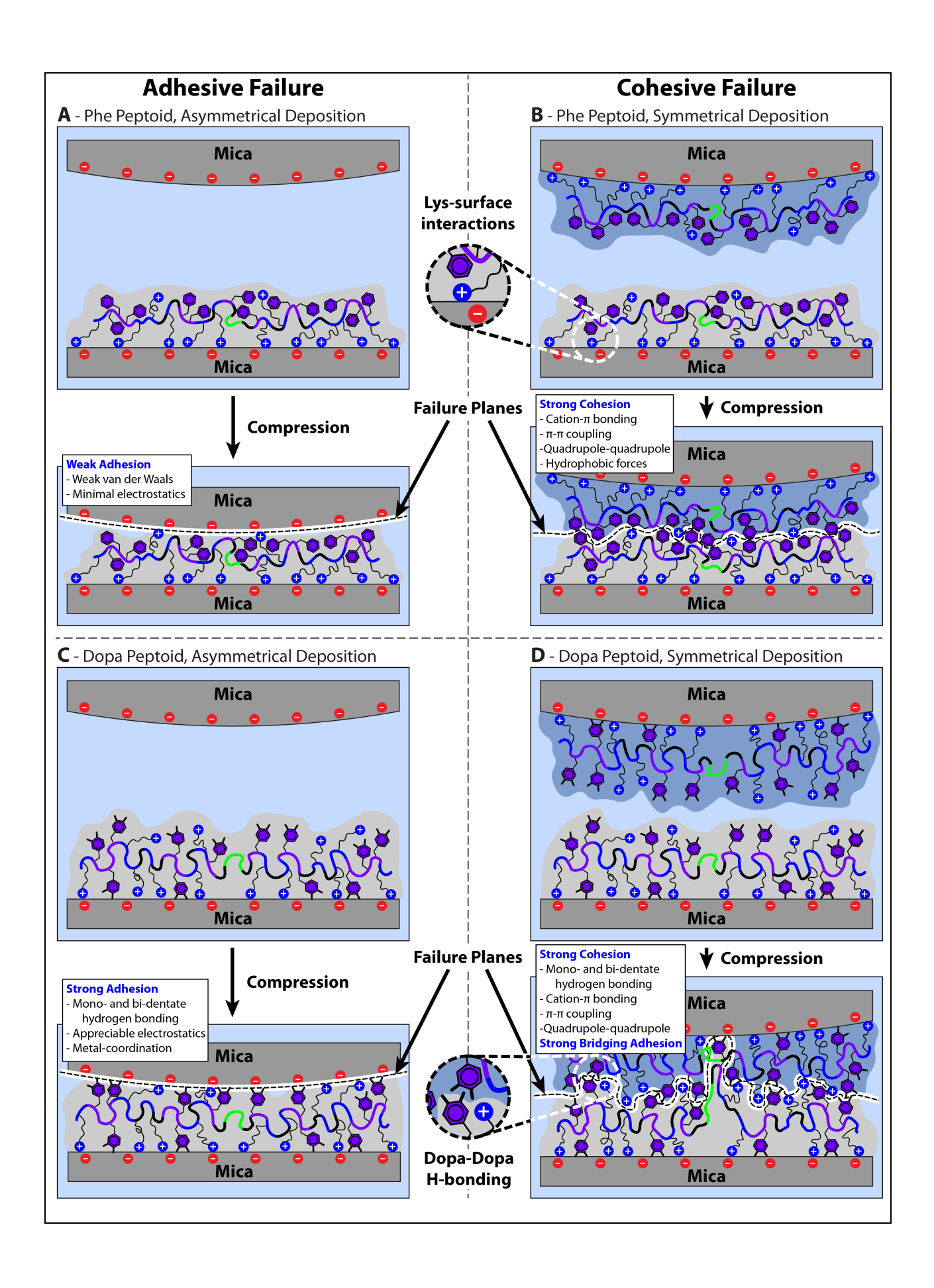


Figure 7. Modeling peptoid adhesion vs. cohesion. Scheme of peptoid films before and after compression for asymmetric deposition of the Phe peptoid (A), symmetric deposition of the Phe peptoid (B), asymmetric deposition of the Dopa peptoid (C), symmetric deposition of the Dopa peptoid (D). In all cases, asymmetrical deposition leads to adhesive failure. Symmetric deposition results in cohesive failure for Phe peptoids (and Tyr peptoids, not depicted) and a combination of cohesive/adhesive failure for Dopa peptoids. Failure planes are indicated by black dashed lines overlaid onto solid white lines. The "boundaries" of each peptoid molecule are indicated with either blue or gray shaded regions. The important interactions at each failure plane are indicated in the white boxes above each 'compressed' pair of surfaces.

#### V. CONCLUSIONS

We have established that mussel-inspired peptoids having high aromatic, lysine, and glycine contents can achieve cohesive strengths comparable with those of analogous peptides and proteins from which they derive. Our investigation has shown that even a subtle change in backbone chemistry can generate profound effects on the behavior and performance of mussel-inspired adhesives. Increased backbone hydrophobicity and inability to form stable secondary structure allow the peptoids to better deposit as thin incompressible films of reduced hydration than peptides of similar sequence. Following asymmetric film deposition, peptoid adhesive strength is positively correlated with increasing ring hydroxylation due to increased flexibility and hydrogen bonding. In symmetric films, the Phe and Tyr peptoids exhibited similar cohesion forces as their peptide analogs. The Dopa peptoid, however, shows greater cohesion than its peptide counterpart due to film dehydration, lower backbone-

mediated intramolecular hydrogen bonding and surface spreading ability. This emphasizes the importance of processing conditions when designing mussel-inspired adhesives.

Peptoid molecules have potential to improve applications for wet adhesion. Though peptides may be classified as 'intrinsically disordered', the backbone chemistry and structure may still influence their molecular properties. If such backbone interactions are undesirable for specific applications, such as selective surface priming, peptoid molecules can be used to maintain side chain function without the complication of backbone interactions. Then, intermolecular ordering can be engineered through specific side-chain interactions to tailor a peptoid structure based on a desired function.

# **Declarations**

Author contributions: WRW proposed the idea of testing peptoid adhesion. WRW synthesized and characterized the peptoids, TRC and GDD performed adhesion tests on the surface forces apparatus, KC and JES parameterized peptoid structures and did simulations, JHW and KES directed and coordinated the research. WRW, TRC, KRC, KC, GDD, JES and JHW analyzed and interpreted the data and wrote the manuscript.

#### **Competing Interests:** None

Supporting Information: The supporting information is available free of charge on the ACS Publications website at DOI:10.1021/acs-macromol. Includes SFA compression and separation forces on bare mica and asymmetric peptides (S1, S2) and modeling data for 2° structure in F, Y and Dopa substituted peptides (S3), structure clusters in peptides and peptoids (S4), Lysine surface proximity (S5), hydroxyl surface proximity (S6), Dopa surface interactions (S7), peptide 2° structure on mica for 20 and 100 ps (S8, S9).

- Availability of Data and Materials: Available upon request
- 2 **Funding:** This research was funded by a National Science Foundation MRSEC grant No.
- 3 DMR 1720256 to the UCSB Materials Research Laboratory of which JES and JHW are IRG3
- 4 investigators. WRW, KEC received IRG3 training support. Additional support for trainees was
- 5 provided through NSF EAGER No. 1508717 (WRW), an NSF Graduate Research Fellowship No.
- 6 1650114 (GDD), and the Department of Energy Grant No. DE-FG02-87ER-45331 (TRC).
- 7 Peptoids were synthesized as User Project at the Molecular Foundry (LBNL), supported by the
- 8 Office of Science, Office of Basic Energy Sciences of the U.S. Department of Energy under
- 9 contract No. DE-AC02-05CH11231. JES acknowledges partial support by NSF Grant # MCB-
- 10 1716956. The research reported here made use of support from the Center for Scientific
- 11 Computing from the CNSI, MRL: an NSF MRSEC (DMR-1720256) and NSF CNS-1725797. JES
- 12 acknowledges support from the Extreme Science and Engineering Discovery Environment—
- 13 XSEDE (TG-MCA05S027) supported by NSF ACI-1053575.
- 14 **ACKNOWLEDGEMENTS**: We recognize Professor Jacob N. Israelachvili, who passed away in
- 15 September 2018, for his enthusiastic involvement in the early stages of this work. We also
- 16 acknowledge the Texas Advanced Computing Center (TACC) at The University of Texas at Austin
- 17 for providing HPC resources that contributed to the research results reported within this paper.

#### References

18

19

1

- 20 (1) Lee, B. P.; Messersmith, P. B.; Israelachvili, J. N.; Waite, J. H. Mussel-Inspired Adhesives and
- 21 Coatings. Annu. Rev. Mater. Res. 2011, 41, 99–132. https://doi.org/10.1146/annurev-matsci-
- 22 062910-100429.

- 1 (2) Floriolli; von Langen J; Waite. Marine Surfaces and the Expression of Specific Byssal Adhesive
- Protein Variants in Mytilus. Mar. Biotechnol. (NY). 2000, 2 (4), 352–363.
- 3 (3) Hofman, A. H.; van Hees, I. A.; Yang, J.; Kamperman, M. Bioinspired Underwater Adhesives by
- 4 Using the Supramolecular Toolbox. *Adv. Mater.* **2018**, *30* (19), 1704640.
- 5 https://doi.org/10.1002/adma.201704640.
- 6 (4) Lee, H.; Scherer, N. F.; Messersmith, P. B. Single-Molecule Mechanics of Mussel Adhesion. *Proc.*
- 7 Natl. Acad. Sci. U. S. A. **2006**, 103 (35), 12999–13003. https://doi.org/10.1073/pnas.0605552103.
- 8 (5) Kord Forooshani, P.; Lee, B. P. Recent Approaches in Designing Bioadhesive Materials Inspired by
- 9 Mussel Adhesive Protein. J. Polym. Sci. Part A Polym. Chem. 2017, 55 (1), 9–33.
- 10 https://doi.org/10.1002/pola.28368.
- 11 (6) Kim, S.; Faghihnejad, A.; Lee, Y.; Jho, Y. S.; Zeng, H.; Hwang, D. S. Cation-π Interaction in DOPA-
- Deficient Mussel Adhesive Protein Mfp-1. J. Mater. Chem. B 2015, 3 (5), 738–743.
- 13 https://doi.org/10.1039/c4tb01646g.
- 14 (7) Das, S.; Rodriguez, N. R. M.; Wei, W.; Waite, J. H.; Israelachvili, J. N. Peptide Length and Dopa
- Determine Iron-Mediated Cohesion of Mussel Foot Proteins; Wiley-Blackwell, 2015; Vol. 25, pp
- 16 5840–5847. https://doi.org/10.1002/adfm.201502256.
- 17 (8) Yu, J.; Wei, W.; Menyo, M. S.; Masic, A.; Waite, J. H.; Israelachvili, J. N. Adhesion of Mussel Foot
- 18 Protein-3 to TiO2 Surfaces: The Effect of PH. *Biomacromolecules* **2013**, *14* (4), 1072–1077.
- 19 https://doi.org/10.1021/bm301908y.
- 20 (9) Rodriguez, N. R. M.; Das, S.; Kaufman, Y.; Israelachvili, J. N.; Waite, J. H. Interfacial PH during
- 21 Mussel Adhesive Plaque Formation. *Biofouling* **2015**, *31* (2), 221–227.
- 22 https://doi.org/10.1080/08927014.2015.1026337.

- 1 (10) Lu, Q.; Danner, E.; Waite, J. H.; Israelachvili, J. N.; Zeng, H.; Hwang, D. S. Adhesion of Mussel Foot
- 2 Proteins to Different Substrate Surfaces. J. R. Soc. Interface 2013, 10 (79).
- 3 https://doi.org/10.1098/rsif.2012.0759.
- 4 (11) Levine, Z. A.; Rapp, M. V; Wei, W.; Mullen, R. G.; Wu, C.; Zerze, G. H.; Mittal, J.; Waite, J. H.;
- 5 Israelachvili, J. N.; Shea, J.-E. Surface Force Measurements and Simulations of Mussel-Derived
- Peptide Adhesives on Wet Organic Surfaces. Proc. Natl. Acad. Sci. 2016, 113 (16), 4332–4337.
- 7 https://doi.org/10.1073/pnas.1603065113.
- 8 (12) Wei, W.; Yu, J.; Gebbie, M. A.; Tan, Y.; Martinez Rodriguez, N. R.; Israelachvili, J. N.; Waite, J. H.
- 9 Bridging Adhesion of Mussel-Inspired Peptides: Role of Charge, Chain Length, and Surface Type.
- 10 Langmuir **2015**, *31* (3), 1105–1112. https://doi.org/10.1021/la504316q.
- 11 (13) Rapp, M. V; Maier, G. P.; Dobbs, H. A.; Higdon, N. J.; Waite, J. H.; Butler, A.; Israelachvili, J. N.
- 12 Defining the Catechol-Cation Synergy for Enhanced Wet Adhesion to Mineral Surfaces. J. Am.
- 13 Chem. Soc. **2016**, 138 (29), 9013–9016. https://doi.org/10.1021/jacs.6b03453.
- 14 (14) Yu, J.; Kan, Y.; Rapp, M.; Danner, E.; Wei, W.; Das, S.; Miller, D. R.; Chen, Y.; Waite, J. H.;
- 15 Israelachvili, J. N. Adaptive Hydrophobic and Hydrophilic Interactions of Mussel Foot Proteins
- 16 with Organic Thin Films. *Proc. Natl. Acad. Sci. U. S. A.* **2013**, *110* (39), 15680–15685.
- 17 https://doi.org/10.1073/pnas.1315015110.
- 18 (15) Hwang, D. S.; Waite, J. H. Three Intrinsically Unstructured Mussel Adhesive Proteins, Mfp-1, Mfp-
- 19 2, and Mfp-3: Analysis by Circular Dichroism. *Protein Science*. 2012, pp 1689–1695.
- 20 https://doi.org/10.1002/pro.2147.
- 21 (16) Gebbie, M. A.; Wei, W.; Schrader, A. M.; Cristiani, T. R.; Dobbs, H. A.; Idso, M.; Chmelka, B. F.;
- Waite, J. H.; Israelachvili, J. N. Tuning Underwater Adhesion with Cation–π Interactions. *Nat.*

- 1 *Chem.* **2017**, *9* (5), 473–479. https://doi.org/10.1038/nchem.2720.
- 2 (17) Kirshenbaum, K.; Barron, A. E.; Goldsmith, R. A.; Armand, P.; Bradley, E. K.; Truong, K. T. V.; Dill, K.
- 3 A.; Cohen, F. E.; Zuckermann, R. N. Sequence-Specific Polypeptoids: A Diverse Family of
- 4 Heteropolymers with Stable Secondary Structure. Proc. Natl. Acad. Sci. U. S. A. 1998, 95 (8),
- 5 4303–4308. https://doi.org/10.1073/pnas.95.8.4303.
- 6 (18) Huang, K.; Wu, C. W.; Sanborn, T. J.; Patch, J. A.; Kirshenbaum, K.; Zuckermann, R. N.; Barron, A.
- 7 E.; Radhakrishnan, I. A Threaded Loop Conformation Adopted by a Family of Peptoid Nonamers.
- 8 J. Am. Chem. Soc. **2006**, 128 (5), 1733–1738. https://doi.org/10.1021/ja0574318.
- 9 (19) Tran, H.; Gael, S. L.; Connolly, M. D.; Zuckermann, R. N. Solid-Phase Submonomer Synthesis of
- 10 Peptoid Polymers and Their Self-Assembly into Highly-Ordered Nanosheets. J. Vis. Exp. 2011, No.
- 11 57. https://doi.org/10.3791/3373.
- 12 (20) Wellings, D. A.; Atherton, E. [4] Standard Fmoc Protocols. In Methods in Enzymology; Academic
- 13 Press, 1997; Vol. 289, pp 44–67. https://doi.org/10.1016/S0076-6879(97)89043-X.
- 14 (21) Israelachvili, J.; Min, Y.; Akbulut, M.; Alig, A.; Carver, G.; Greene, W.; Kristiansen, K.; Meyer, E.;
- Pesika, N.; Rosenberg, K.; Zeng, H. Recent Advances in the Surface Forces Apparatus (SFA)
- 16 Technique. Reports Prog. Phys. **2010**, 73 (3), 036601. https://doi.org/10.1088/0034-
- 17 4885/73/3/036601.
- 18 (22) Johnson, K. L.; Kendall, K.; Roberts, A. D. Surface Energy and the Contact of Elastic Solids. *Proc. R.*
- 19 *Soc. A Math. Phys. Eng. Sci.* **1971**, *324* (1558), 301–313. https://doi.org/10.1098/rspa.1971.0141.
- 20 (23) Van Der Spoel, D.; Lindahl, E.; Hess, B.; Groenhof, G.; Mark, A. E.; Berendsen, H. J. C. GROMACS:
- 21 Fast, Flexible, and Free. *Journal of Computational Chemistry*. 2005.
- 22 https://doi.org/10.1002/jcc.20291.

- 1 (24) Oostenbrink, C.; Villa, A.; Mark, A. E.; Van Gunsteren, W. F. A Biomolecular Force Field Based on
- the Free Enthalpy of Hydration and Solvation: The GROMOS Force-Field Parameter Sets 53A5 and
- 3 53A6. *J. Comput. Chem.* **2004**, *25* (13), 1656–1676. https://doi.org/DOI 10.1002/jcc.20090.
- 4 (25) Dequidt, A.; Devemy, J.; Malfreyt, P. Confined KCl Solution between Two Mica Surfaces:
- 5 Equilibrium and Frictional Properties. J. Phys. Chem. C 2015, 119 (38), 22080–22085.
- 6 https://doi.org/10.1021/acs.jpcc.5b06880.
- 7 (26) Heinz, H.; Koerner, H.; Anderson, K. L.; Vaia, R. A.; Farmer, B. L. Force Field for Mica-Type Silicates
- 8 and Dynamics of Octadecylammonium Chains Grafted to Montmorillonite. *Chem. Mater.* **2005**.
- 9 https://doi.org/10.1021/cm0509328.
- 10 (27) Bayly, C. I.; Cieplak, P.; Cornell, W.; Kollman, P. A. A Well-Behaved Electrostatic Potential Based
- 11 Method Using Charge Restraints for Deriving Atomic Charges: The RESP Model. *J. Phys. Chem.*
- 12 **1993**, 97 (40), 10269–10280. https://doi.org/10.1021/j100142a004.
- 13 (28) Valiev, M.; Bylaska, E. J.; Govind, N.; Kowalski, K.; Straatsma, T. P.; Van Dam, H. J. J.; Wang, D.;
- Nieplocha, J.; Apra, E.; Windus, T. L.; de Jong, W. A. NWChem: A Comprehensive and Scalable
- 15 Open-Source Solution for Large Scale Molecular Simulations. *Comput. Phys. Commun.* **2010**, *181*
- 16 (9), 1477–1489. https://doi.org/http://dx.doi.org/10.1016/j.cpc.2010.04.018.
- 17 (29) Das, S.; Lee, B. H.; Linstadt, R. T.; Cunha, K.; Li, Y.; Kaufman, Y.; Levine, Z. A.; Lipshutz, B. H.; Lins,
- 18 R. D.; Shea, J. E.; Heeger, A. J.; Ahn, B. K. Molecularly Smooth Self-Assembled Monolayer for High-
- 19 Mobility Organic Field-Effect Transistors. *Nano Lett* **2016**, *16* (10), 6709–6715.
- 20 https://doi.org/10.1021/acs.nanolett.6b03860.
- 21 (30) Berendsen, H. J. C.; Postma, J. P. M.; van Gunsteren, W. F.; Hermans, J. Intermolecular Forces.
- 22 Pullman, B., Ed.; Reidel Publ. Co. Dordr. 1981, 331–342.

- 1 https://doi.org/papers2://publication/livfe/id/165650.
- 2 (31) Hess, B.; Bekker, H.; Berendsen, H. J. C.; Fraaije, J. G. E. M. LINCS: A Linear Constraint Solver for
- 3 Molecular Simulations. *J. Comput. Chem.* **1997**, *18* (12), 1463–1472.
- 4 https://doi.org/papers2://publication/livfe/id/165645.
- 5 (32) Hockney, R. W. The Potential Calculation and Some Applications. In *Methods in Computational*
- 6 Physics; Alder, B., Fernbach, S., Rotenberg, M., Eds.; Academic Press: New York/London, 1970;
- 7 Vol. 9.
- 8 (33) Darden, T.; York, D.; Pedersen, L. Particle Mesh Ewald: An N·log(N) Method for Ewald Sums in
- 9 Large Systems. *J. Chem. Phys.* **1993**, *98* (12), 10089–10092.
- 10 https://doi.org/doi:http://dx.doi.org/10.1063/1.464397.
- 11 (34) Hoover, W. G. Canonical Dynamics: Equilibrium Phase-Space Distributions. *Phys. Rev. A* 1985.
- 12 https://doi.org/10.1103/PhysRevA.31.1695.
- 13 (35) Parrinello, M.; Rahman, A. Polymorphic Transitions in Single Crystals: A New Molecular Dynamics
- 14 Method. J. Appl. Phys. **1981**. https://doi.org/10.1063/1.328693.
- 15 (36) Nosé, S.; Klein, M. L. Constant Pressure Molecular Dynamics for Molecular Systems. *Mol. Phys.*
- 16 **1983**. https://doi.org/10.1080/00268978300102851.
- 17 (37) Daura, X.; Gademann, K.; Schäfer, H.; Jaun, B.; Seebach, D.; Van Gunsteren, W. F. The β-Peptide
- 18 Hairpin in Solution: Conformational Study of a β-Hexapeptide in Methanol by NMR Spectroscopy
- 19 and MD Simulation. J. Am. Chem. Soc. **2001**. https://doi.org/10.1021/ja003689g.
- 20 (38) Kabsch, W.; Sander, C. Dictionary of Protein Secondary Structure: Pattern Recognition of
- 21 Hydrogen-bonded and Geometrical Features. *Biopolymers* **1983**.
- 22 https://doi.org/10.1002/bip.360221211.

- 1 (39) Touw, W. G.; Baakman, C.; Black, J.; Te Beek, T. A. H.; Krieger, E.; Joosten, R. P.; Vriend, G. A
- 2 Series of PDB-Related Databanks for Everyday Needs. *Nucleic Acids Res.* **2015**.
- 3 https://doi.org/10.1093/nar/gku1028.
- 4 (40) Humphrey, W.; Dalke, A.; Schulten, K. VMD: Visual Molecular Dynamics. J. Mol. Graph. 1996.
- 5 https://doi.org/10.1016/0263-7855(96)00018-5.
- 6 (41) Micsonai, A.; Wien, F.; Kernya, L.; Lee, Y. H.; Goto, Y.; Réfrégiers, M.; Kardos, J. Accurate
- 7 Secondary Structure Prediction and Fold Recognition for Circular Dichroism Spectroscopy. *Proc.*
- 8 *Natl. Acad. Sci. U. S. A.* **2015**, *112* (24), E3095–E3103. https://doi.org/10.1073/pnas.1500851112.
- 9 (42) Waite, J. H.; Qin, X. Polyphosphoprotein from the Adhesive Pads of Mytilus Edulis. *Biochemistry*
- 10 **2001**. https://doi.org/10.1021/bi002718x.
- 11 (43) Maier, G. P.; Rapp, M. V.; Waite, J. H.; Israelachvili, J. N.; Butler, A. Adaptive Synergy between
- 12 Catechol and Lysine Promotes Wet Adhesion by Surface Salt Displacement. Science (80-. ). 2015,
- 13 349 (6248), 628–632. https://doi.org/10.1126/science.aab0556.
- 14 (44) Israelachvili, J. N. Intermolecular and Surface Forces: Revised Third Edition; Academic Press, 2011;
- Vol. 33. https://doi.org/10.1073/pnas.0703993104.
- 16 (45) Sedő, J.; Saiz-Poseu, J.; Busqué, F.; Ruiz-Molina, D. Catechol-Based Biomimetic Functional
- 17 Materials. Adv. Mater. 2013, 25 (5), 653–701. https://doi.org/10.1002/adma.201202343.
- 18 (46) Pinnaratip, R.; Bhuiyan, M. S. A.; Meyers, K.; Rajachar, R. M.; Lee, B. P. Multifunctional Biomedical
- 19 Adhesives. Adv. Healthc. Mater. **2019**, 8 (11), 1–17. https://doi.org/10.1002/adhm.201801568.
- 20 (47) Degen, G. D.; Stow, P. R.; Lewis, R. B.; Andresen Eguiluz, R. C.; Valois, E.; Kristiansen, K.; Butler, A.;
- 21 Israelachvili, J. N. Impact of Molecular Architecture and Adsorption Density on Adhesion of
- 22 Mussel-Inspired Surface Primers with Catechol-Cation Synergy. J. Am. Chem. Soc. 2019.

- 1 https://doi.org/10.1021/jacs.9b04337.
- 2 (48) Ahn, B. K.; Lee, D. W.; Israelachvili, J. N.; Waite, J. H. Surface-Initiated Self-Healing of Polymers in
- 3 Aqueous Media. *Nat. Mater.* **2014**, *13* (9), 867–872. https://doi.org/10.1038/nmat4037.
- 4 (49) Ahn, B. K.; Das, S.; Linstadt, R.; Kaufman, Y.; Martinez-Rodriguez, N. R.; Mirshafian, R.; Kesselman,
- 5 E.; Talmon, Y.; Lipshutz, B. H.; Israelachvili, J. N.; Waite, J. H. High-Performance Mussel-Inspired
- 6 Adhesives of Reduced Complexity. *Nat. Commun.* **2015**, *6*, 1–7.
- 7 https://doi.org/10.1038/ncomms9663.
- 8 (50) Truex, N. L.; Nowick, J. S. Coassembly of Peptides Derived from β-Sheet Regions of β-Amyloid. J.
- 9 Am. Chem. Soc. **2016**, 138 (42), 13891–13900. https://doi.org/10.1021/jacs.6b06001.
- 10 (51) Chiti, F.; Stefani, M.; Taddei, N.; Ramponi, G.; Dobson, C. M. Rationalization of the Effects of
- Mutations on Peptide and Protein Aggregation Rates. *Nature* **2003**, *424* (6950), 805–808.
- 12 https://doi.org/10.1038/nature01891.
- 13 (52) Yu, J.; Wei, W.; Danner, E.; Israelachvili, J. N.; Waite, J. H. Effects of Interfacial Redox in Mussel
- 14 Adhesive Protein Films on Mica. *Adv. Mater.* **2011**, *23* (20), 2362–2366.
- 15 https://doi.org/10.1002/adma.201003580.
- 16 (53) Miller, D. R.; Spahn, J. E.; Waite, J. H. The Staying Power of Adhesion-Associated Antioxidant
- 17 Activity in Mytilus Californianus. J. R. Soc. Interface 2015, 12 (111), 20150614.
- 18 https://doi.org/10.1098/rsif.2015.0614.
- 19 (54) Waite, J. H. Mussel Adhesion Essential Footwork. J. Exp. Biol. 2017, 220 (4), 517–530.
- 20 https://doi.org/10.1242/jeb.134056.
- 21 (55) Wei, W.; Yu, J.; Broomell, C.; Israelachvili, J. N.; Waite, J. H. Hydrophobic Enhancement of Dopa-
- Mediated Adhesion in a Mussel Foot Protein. Journal of the American Chemical Society. 2013, pp

